Optimum Design of Dye-Sensitized Solar Module for Building-Integrated Photovoltaic Systems

Kyu-Seok Lee and Man Gu Kang

This paper presents a method for determining the optimum active-area width (OAW) of solar cells in a module architecture. The current density–voltage curve of a reference cell with a narrow active-area width is used to reproduce the current density profile in the test cell whose active area width is to be optimized. We obtained self-consistent current density and electric potential profiles from iterative calculations of both properties, considering the distributed resistance of the contact layers. Further, we determined the OAW that yields the maximum efficiency by calculating efficiency as a function of the active-area width. The proposed method can be applied to the design of the active area of a dye-sensitized solar cell in Z-type series connection modules for indoor and building-integrated photovoltaic systems. Our calculations predicted that OAW increases as the sheet resistances of the contact layers and the intensity of light decrease.

Keywords: Current density–voltage curve, Dye-sensitized solar cell, Optimum active-area width, Z-type series connection.

I. Introduction

Dye-sensitized solar cells (DSCs) have been extensively studied owing to their application in indoor and building-integrated photovoltaic (BIPV) systems [1]–[5]. These cells have certain advantages, including an abundance of materials, a simple fabrication process [6], [7], low production cost [8]–[10], various colors, high transparency, and a better performance compared with other devices under diffused lighting conditions [11]. Most previous studies on DSCs focus on improving cell performance [12]–[15]. The active-area efficiency of a solar cell is often defined as the maximum output electric power against the input power of 1-sun AM 1.5G illumination on a designated active area. With the development of efficient dyes and electrodes with high catalytic activity, the certified efficiency of DSC has reached 11.9% with an active area of 1.005 cm^2 [13], [16]. Recently, improving the module performance has gained increasing attention [17]–[27].

Given that the solar cell in the module architecture has active and interconnection areas, the conversion efficiency of the module with respect to the total area equals the product of the active-area efficiency of the unit cell and the ratio of the active area against the total area of the cell [25]. Since the active-area efficiency and the geometrical ratio reveal competing behaviors with varying widths in the active-area, there is an optimum active-area width (OAW) that yields the maximum efficiency with minimum loss in output power.

In previous studies [26] and [27], the width of the active area of a solar cell was optimized by calculating power loss from several factors such as interconnection area, contact-layer (window-layer) absorption, and contact-layer sheet resistance. For small power losses, the fraction of power lost owing to the window-layer sheet resistance was

Manuscript received Jan. 16, 2017; revised Aug. 23, 2017; accepted Sept. 11, 2017.

Kyu-Seok Lee (corresponding author, kyulee@etri.re.kr) and Man Gu Kang (1009kang@etri.re.kr) are with the ICT Materials & Components Research Laboratory, ETRI, Daejeon, Rep. of Korea.

estimated based on Joule heating losses, assuming a uniform current density. However, for large power losses, such an assumption does not hold. To work around this problem, Rowell and McGehee used distributed diode models [26].

In this paper, we present a method to determine the OAW of solar cells in a module architecture. The current density–voltage curve (J–V) of a small-sized reference cell is used to calculate the average current density of the test cell whose active-area width is to be optimized. The characteristic parameters of the reference cell are extracted by fitting with a J–V curve. Using these parameters and considering the distributed resistance of the contact layers [28], [29], we calculate the efficiency of the test cell as a function of the active-area width, and we determine the OAW that yields the maximum efficiency. The proposed method is applied to the design of the active area of the DSCs in a Z-type series connection for indoor and BIPV systems. The dependence of the OAW on sheet resistances of the contact layers and the intensity of light is discussed.

II. Formalism

The reference and test cells have the same structure, which consists of a front contact layer, an active layer (or active media), and a rear contact layer. The test cell is in a Z-type series connection and has active and interconnection areas with widths a and d, respectively, and a common length L. The schematic cross-section of the active area of the test cell is shown in Fig. 1. The

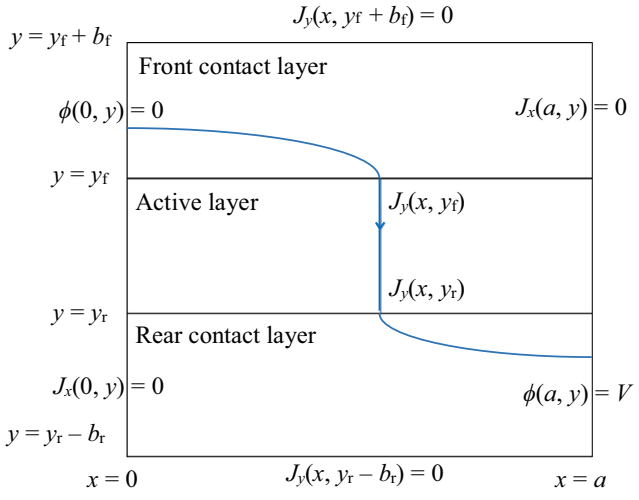

Fig. 1. Schematic cross section of the active area of a cell in a Z-type series connection. Boundary conditions for the Laplace equation are specified at all boundaries of the front and rear contact layers.

reference cell has a narrow active-area width a_{ref}, and thus, its contact layers are assumed to have constant specific resistances.

Under illumination, an electric current is generated in the test cell at a bias voltage of V between the right edge ($x = a$) of the rear contact layer and the left edge ($x = 0$) of the front contact layer. Under voltages less than the open-circuit voltage, the current exits from the rear contact layer. For most solar cells, the active layer has a much smaller conductivity than that of both contact layers. For instance, the conductivity of a solvent electrolyte in the active layer of DSCs is ~0.01 S/cm, whereas the conductivity of a typical fluorine-doped tin oxide (FTO) with 2.5% fluorine, used as a material for the contact layer of DSCs, is ~1.5×10^3 S/cm [30]. Thus, the current passing through the active-layer/contact-layer interfaces has only the y-component, $J(x)$.

Electric potentials in the front and rear contact layers can be calculated from the Laplace equation with the boundary conditions specified in Fig. 1. The electric potential difference $V_a(x)$ between the rear and front boundaries of the active layer under a bias voltage V is written as [29].

$$V_a(x) = V - \sum_{n=1}^{\infty} \{A_{f,n} \sin(\lambda_n x) + A_{r,n} \sin(\lambda_n x')\}, \quad (1)$$

where $\lambda_n = (2n-1)\pi/2a, x' = a - x$,

$$A_{f,n} = \frac{4 \coth(\lambda_n b_f)}{\pi \sigma_f (2n-1)} \int_0^a J(x) \sin(\lambda_n x) dx, \quad (2)$$

and

$$A_{r,n} = \frac{4 \coth(\lambda_n b_r)}{\pi \sigma_r (2n-1)} \int_0^a J(x) \sin(\lambda_n x') dx. \quad (3)$$

Here, b_f (σ_f) and b_r (σ_r) denote the thickness (conductivities) of the front and rear contact layers, respectively.

To calculate $A_{f,n}$ and $A_{r,n}$ in (2) and (3) analytically, we write $J(x)$ in terms of a constant and $2m$ sine functions in (1) [29].

$$J(x) = J_0 + \sum_{n=1}^{m} \{c_{f,n} \sin(\lambda_n x) + c_{r,n} \sin(\lambda_n x')\}, \quad (4)$$

where J_0 is the current density in the ideal cell that has the same structure as the test cell, but has both contact layers of zero sheet resistances. The other terms represent the perturbation of the current density owing to the resistive contact layers. Here, $c_{f,n}$ and $c_{r,n}$ are the expansion coefficients of the perturbed terms.

https://doi.org/10.4218/etrij.2017-0088

Because $a \gg b_f$ and $a \gg b_r$, $V_a(x)$ is written as [29]

$$V_a(x) = V - \frac{J_0}{2}\left[r_f x(2a-x) + r_r(a^2-x^2)\right] - \sum_{n=1}^{m}\left[B_{f,n}\sin(\lambda_n x) + B_{r,n}\sin(\lambda_n x')\right], \quad (5)$$

where

$$B_{f,n} = \frac{4a^2 r_f}{\pi^3(2n-1)^2}\left[\pi c_{f,n} + \frac{2c_{r,n}(-1)^{n+1}}{2n-1} + \sum_{k\neq n}^{m} c_{r,k}\frac{(2n-1)(-1)^k - (2k-1)(-1)^n}{(k+n-1)(k-n)}\right] \quad (6)$$

and

$$B_{r,n} = \frac{4a^2 r_r}{\pi^3(2n-1)^2}\left[\pi c_{r,n} + \frac{2c_{f,n}(-1)^{n+1}}{2n-1} + \sum_{k\neq n}^{m} c_{f,k}\frac{(2n-1)(-1)^k - (2k-1)(-1)^n}{(k+n-1)(k-n)}\right]. \quad (7)$$

Here, $r_f = 1/b_f\sigma_f$ and $r_r = 1/b_r\sigma_r$, representing the sheet resistances of the front and rear contact layers, respectively. In addition, $c_{f,n}$ and $c_{r,n}$ can be determined from independent $2m$ linear equations constructed from (4) at $2m$ positions of $x = x_p$ for $p = 1, 2, \ldots, 2m$ [29]. We chose $m = 10$ and $x_p = (p-1)a/(2m-1)$ for all calculations presented in this paper.

In the present approach, J_0 and $J(x_p)$ for $p = 1, 2, \ldots, 2m$ are reproduced from a measured J–V curve of the reference cell. The J–V curve is fitted with that of a single-diode model, the equivalent circuit of which is depicted in Fig. 2. The J–V relationship of the single-diode model is written as

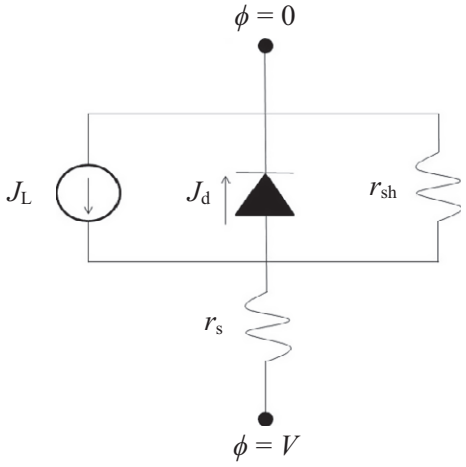

Fig. 2. Equivalent circuit of the solar cell.

$$V - Jr_s - r_{sh}[J + J_L - J_d] = 0, \quad (8)$$

where $J_d = J_s[\exp\{q(V - Jr_s)/\xi kT\} - 1]$. Here q, k, and T are the elementary charge, Boltzmann constant, and temperature in kelvin, respectively. In addition, J_L, J_d, J_s, ξ, r_{sh}, and r_s denote the photocurrent density, diode current density, reverse saturation current density, ideality factor, specific shunt resistance, and specific series resistance, respectively.

The single-diode model may not represent the mechanism of the photovoltaic phenomena in DSCs [31], [32]. However, in the present formalism, an accurate reproduction of the measured J–V curve is critical. The single-diode model is employed to reproduce the current density profile in the test cell using a numerical fit with the J–V curve of the reference cell. The specific series resistance of the active layer is estimated from the relation $r_{s,A} = r_{s,ref} - r_{s,C,ref}$, where $r_{s,ref}$ and $r_{s,C,ref}$ denote the specific series resistances of the reference cell and its contact layers, respectively. In addition, $r_{s,ref}$ is extracted from the fit, and $r_{s,C,ref}$ is approximated as $r_{s,C,ref} \approx a^2{}_{ref}(r_f + r_r)/3$.

Here, the J_0 of the ideal cell can be reproduced from (8) using $r_s = r_{s,A}$ and other characteristic parameters of the reference cell. In addition, $J(x_p)$ of the test cell is equivalent to the current density in the ideal cell at a bias voltage of $V = V_a(x_p)$. Initially, $J(x_p)$ and $V_a(x_p)$ for $p = 1, 2, \ldots, 2m$ may be calculated with $c_{f,n} = c_{r,n} = 0$ for $n = 1, 2, \ldots, m$. Consistent results for $c_{f,n}$ and $c_{r,n}$ are obtained from iterative calculations of $V_a(x_p)$ and $J(x_p)$. Subsequently, the average current density is obtained from the following equation, which was derived from (4).

$$J_a = J_0 + \frac{2}{\pi}\sum_{n=1}^{m}\frac{c_{f,n} + c_{r,n}}{2n-1}. \quad (9)$$

The efficiency of a solar cell in a Z-type series connection is written as [25]

$$\eta = \frac{a}{a+d}\eta_a. \quad (10)$$

Here, $\eta_a = P_m/P_i$ denotes the active-area efficiency; P_i is the power density of the light; $P_m = J_m V_m = \max(J_a V)$ represents the maximum output power density; and J_m and V_m denote the current density and bias voltage at the maximum power point, respectively.

III. Application to Dye-Sensitized Solar Cells

Let us apply the proposed method to determine the OAW of the DSCs in a Z-type series connection where the front and rear contact layers have the same sheet

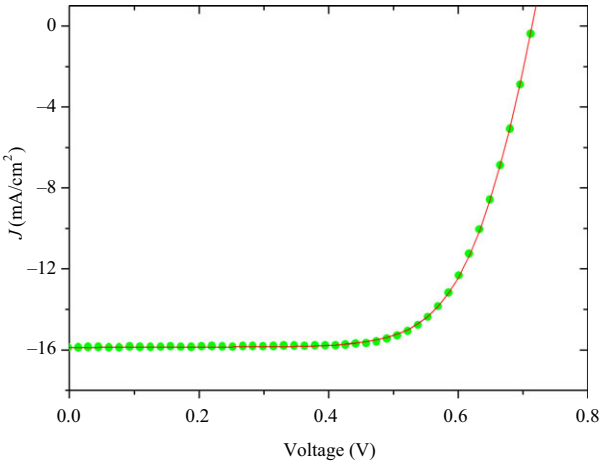

Fig. 3. Fitting (line) with the *J–V* curve (closed circles) of the reference cell using a single-diode model.

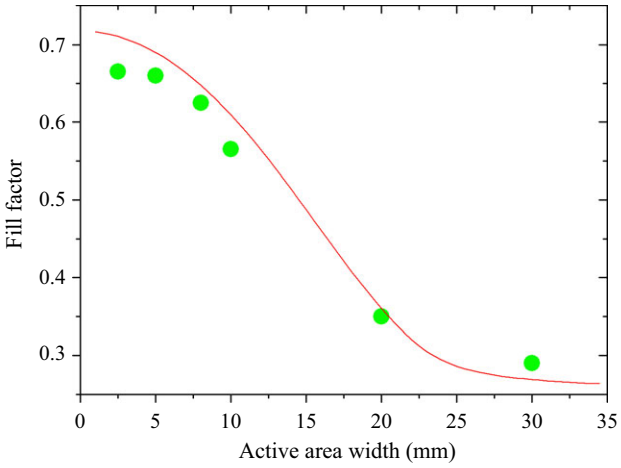

Fig. 4. FF versus active-area width. The closed circles and solid line represent the experimental and calculated results, respectively.

resistance. The fabrication of the DSCs for this study was detailed elsewhere [33], [34]. The reference cell had an active area of 0.4 × 0.5 cm^2. The p- and n-contact pads were formed at two opposite sides of the active area with a gap of ~0.4 cm. The sheet resistances of both contact layers were $r_f = r_r = 9$ Ω/sq. The *J–V* curve of the reference cell was measured at room temperature, using a solar simulator equipped with Keithley 2400 source meter and a 1,000 W Xenon lamp (Oriel, 91193) that provided illumination approximating 1-sun light of AM 1.5G.

Figure 3 shows the fitting with the *J–V* curve of the reference cell using a calculation through (8). From this fitting, we obtained $r_{s,ref} = 3.048 \times 10^{-4}$ Ωm^2, $r_{sh} = 1.145$ Ωm^2, $J_s = 8.694 \times 10^{-5}$ A/m^2, $J_L = 158.8$ A/m^2, and $\xi = 1.9164$. With $r_f = r_r = 9$ Ω/sq, we have $r_{s,C,ref} \approx a^2_{ref}\ (r_f + r_r)/3 = 0.96 \times 10^{-4}$ Ωm^2 and $r_{s,A} = r_{s,ref} - r_{s,C,ref} \approx 2.088 \times 10^{-4}$ Ωm^2. Using $r_{s,A}$ and other characteristic parameters of the reference cell, we calculated J_0 in the ideal cell and $J(x_p)$ in the active layer of the test cell at $x_p = (p - 1)a/19$ for $p = 1, 2, \ldots, 20$ under a bias voltage V. Computing J_a as a function of the bias voltage, we determined the various properties of the test cells such as fill factor (FF), efficiency, and OAW.

Figure 4 shows the FF of the *J–V* curve of DSCs that have the same structure as the reference cell; however, they have various active-area widths. The length and width of the active area were $L = 10$ cm and $a = 2.5$ mm, 5 mm, 8 mm, 10 mm, 20 mm, and 30 mm. The experimental data in the closed circles were reproduced from Fig. 3 in [34]. The calculated results in the solid line are in good agreement with the measured data. As the active-area width increases, the FF decreases and converges to 0.25, which is the FF of a linear *J–V* curve.

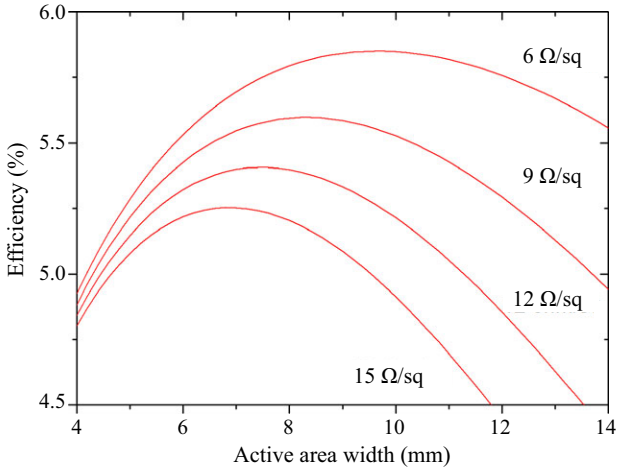

Fig. 5. Efficiency versus active-area width for various contact-layer sheet resistances.

We also determined the OAW of DSCs with various sheet resistances of the contact layers. Figure 5 displays the calculated efficiency versus the active-area width of DSCs whose interconnection-area width was $d = 2.5$ mm and $r_f = r_r = 6$ Ω/sq, 9 Ω/sq, 12 Ω/sq, and 15 Ω/sq. The sheet resistance of each contact layer was assumed to be varied only in terms of its resistivity. The calculated results show that both the OAW and the maximum efficiency increase as the sheet resistances of the contact layers decrease. For $r_f = r_r = 6$ Ω/sq, 9 Ω/sq, 12 Ω/sq, and 15 Ω/sq, OAWs are found to be 9.6 mm, 8.4 mm, 7.4 mm, and 6.8 mm with maximum efficiencies of 5.85%, 5.60%, 5.41%, and 5.25%, respectively. The relative increase in efficiency with decreasing sheet resistances of both contact layers is significant. This result

https://doi.org/10.4218/etrij.2017-0088

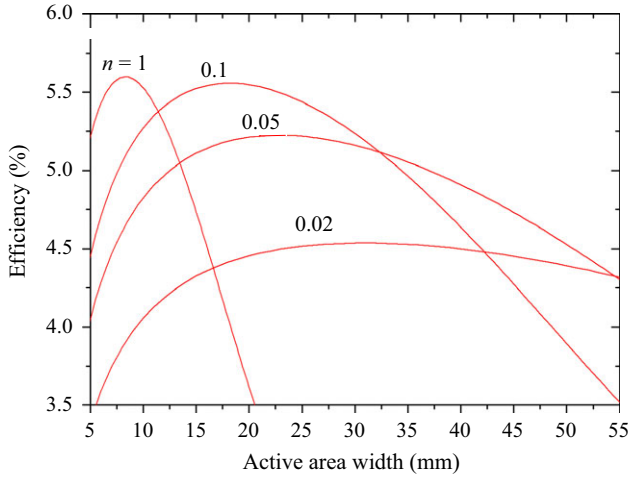

Fig. 6. Efficiency versus active-area width at various n-sun illumination: n = 1, 0.1, 0.05, and 0.02.

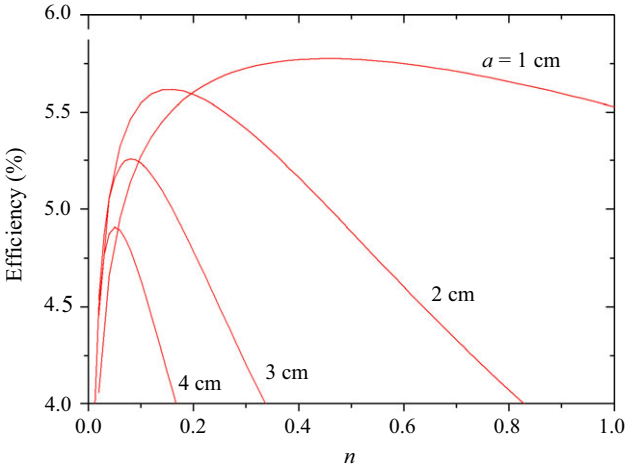

Fig. 7. Efficiency versus n-sun illumination for various active-area widths.

demonstrates that contact layers with low sheet resistances play an important role in improving the efficiency of solar cell modules.

Figure 6 depicts the calculated efficiencies of cells with d = 2.5 mm and $r_f = r_r$ = 9 Ω/sq as a function of the active-area width at various n-sun illumination with $n \leq 1$. With these calculations, we assumed that $J_L = 158.8 \times n$ A/m^2 and that the other characteristic parameters are independent of the light intensity. For n = 1, 0.1, 0.05, and 0.02, OAWs are found to be 8.4 mm, 18 mm, 23 mm, and 31 mm, respectively. OAW is large for a small n. This result may be explained by the fact that η_a is a decreasing function of the active-area width (a), and for an arbitrary a, $|d\eta_a/da|$ increases with n, leading to a decrease in the active-area width that satisfies the condition $d\eta/da = 0$ for the maximum efficiency. Our calculations also show that, for a small n, the efficiency changes minimally from the maximum value in a large range of active-area widths. These results imply that the DSCs for indoor photovoltaic systems can have larger active-area widths in a broad range compared to other cells for outdoor systems.

Figure 7 displays the efficiency versus n-sun illumination for different active-area widths. For a = 10 mm, 20 mm, 30 mm, and 40 mm, the efficiency is at maximum at n = 0.46, 0.16, 0.08, and 0.05, respectively. For large active-area widths, the values of n required to achieve the maximum efficiency are small. This result may be explained as follows. As n increases from zero, the shape of the J–V curve changes from a linear to a rectangular shape, and FF increases. Beyond its maximum, the FF decreases, and the open-circuit voltage, V_{oc}, increases sub-linearly with n, whereas the short-circuit current density, J_{sc}, increases linearly with n. These behaviors of the FF, V_{oc}, and J_{sc} lead to a net decrease in the active-area efficiency. FF falls sharply as active-area width increases, resulting in a decrease in the optimum n required to achieve the maximum active-area efficiency from the cell. Because the efficiency is written as (10), it is at maximum at the same n with the active-area efficiency.

Although not discussed in this paper, the J–V curve of the test cell can also be calculated using a constant resistance model. With this model, the sum of the specific resistance of the front and rear contact layers of the test cell is approximated with $r_{s,C} \approx a^2(r_f + r_r)/3$. Thus, the specific series resistance of the test cell is written as $r_s \approx r_{s,ref} + (a^2 - a^2_{ref})(r_f + r_r)/3$. The J–V curve of the test cell is obtained from (8) using this constant value of r_s and other characteristic parameters of the reference cell. For the DSCs examined in this study, the constant resistance model predicted similar results of the OAW with the proposed method, indicating that the effect of the distributed resistance of the contact layer on the J–V curve was not significant for the DSCs. This result can also be explained from the calculated profiles of $J(x)$ and $V_a(x)$, both of which showed rather weak non-uniformity at a bias voltage of the maximum output power. However, for solar cells with large values of r_f, r_r, and J_L, $J(x)$ and $V_a(x)$ profiles may show a strong non-uniformity. In such cases, the constant resistance model may predict incorrect efficiencies for large active-area widths.

IV. Conclusions

In this paper, a method for designing the OAW of solar cells in a Z-type series connection was presented. The J–V curve of a reference cell was used to reproduce

the density of the current generated in the active area of a test cell. The *J–V* relation derived from a single-diode model was employed for a fitting with the measured *J–V* curve of the reference cell and for calculating the current density in the test cell using the characteristic parameters extracted from the fitting. Considering the distributed resistance of the contact layers, we calculated the consistent current density and electric potential profiles along the active-layer interface. Calculating the efficiency as a function of the active-area width, we determined the OAW with the maximum efficiency. For DSCs with various active-area widths, the calculated FFs were in good agreement with experimental findings. We also found that the OAW of DSCs for indoor and BIPV modules increases as the sheet resistances of both contact layers and the illumination power density decrease.

The proposed method can also be applied to thin film solar cells in monolithic series interconnection, which may be the subject of further studies.

Acknowledgements

This work was supported by the Institute for Information & Communications Technology Promotion (IITP) grant funded by the Korean government (MSIP) (No. B0117-16-1004), and the New Renewable Energy R&D Program of the Korea Institute of Energy Technology Evaluation and Planning (KETEP) grant, also funded by the Korean government (MOTIE) (No. 20163010012470).

References

[1] B.Ò. Regan and M. Grätzel, "A Low-Cost, High-Efficiency Solar Cell Based on Dye-Sensitized Colloidal TiO_2 Films," *Nature*, vol. 353, no. 6346, 1991, pp. 737–740.

[2] M. Grätzel, "Conversion of Sunlight to Electric Power by Nanocrystalline Dye-Sensitized Solar Cells," *J. Photochem. Photobiol. A: Chem.*, vol. 164, 2004, pp. 3–14.

[3] A. Hinsch et al., "Dye Solar Modules for Facade Applications: Recent Results from Project ColorSol," *Sol. Energy Mater. Sol. Cells*, vol. 93, 2009, pp. 820–824.

[4] A. Fakharuddin et al., "A Perspective on the Production of Dye-Sensitized Solar Modules," *Energy Environ. Sci.*, vol. 7, 2014, pp. 3952–3981.

[5] C. Cornaro et al., "Comparative Analysis of the Outdoor Performance of a Dye Solar Cell Mini-Panel for Building Integrated Photovoltaics Applications," *Prog. Photovolt: Res. Appl.*, vol. 23, 2015, pp. 215–225.

[6] T.-C. Wei et al., "Fabrication of Grid Type Dye Sensitized Solar Modules with 7% Conversion Efficiency by Utilizing Commercially Available Materials," *Prog. Photovolt: Res. Appl.*, vol. 21, 2013, pp. 1625–1633.

[7] G.E. Tulloch, "Light and Energy — Dye Solar Cells for the 21st Century," *J. Photochem. Photobiol. A: Chem.*, vol. 164, 2004, pp. 209–219.

[8] L. Vesce et al., "Optimization of Nanostructured Titiania Photoanodes for Dye-Sensitized Solar Cells: Study and Experimentation of $TiCl_4$ Treatment," *J. Non-Cryst. Solids*, vol. 356, 2010, pp. 1958–1961.

[9] L. Vesce and R. Riccitelli, "Processing and Characterization of a TiO_2 Paste Based on Small Particle Size Powders for Dye-Sensitized Solar Cell Semi-Transparent Photo-Electrodes," *Prog. Photovolt: Res. Appl.*, vol. 20, 2012, pp. 960–966.

[10] G. Mincuzzi et al., "Taking Temperature Processing out of Dye-Sensitized Solar Cell Fabrication: Fully Laser Manufactured Devices," *Adv. Energy Mater.*, vol. 4, no. 14, May 2014, pp. 1400421:1–1400421:8.

[11] N. Sridhar and D. Freeman, "A Study of Dye Sensitized Solar Cells under Indoor and Low Level Outdoor Lighting: Comparision to Organix and Inorganic Thin Film Solar Cells and Methods to Address Maximum Power Point Tracking," *Eur. Photovolt. Solar Energy Conf. Exhibit.*, Hamburg, Germany, 2011, pp. 232–236.

[12] S. Ito et al., "High Efficiency Organic-Dye-Sensitized Solar Cells Controlled by Nanocrystalline-TiO_2 Electrode Thickness," *Adv. Mater.*, vol. 18, 2006, pp. 1202–1205.

[13] R. Komiya et al., "Improvement of the Conversion Efficiency of a Monolithic Type Dye-Sensitized Solar Cell Module," *Techn. Digest, Int. Photovoltaic Sci. Eng. Conf.*, Fukuoka, Japan, Nov. 2011, p. 2C-5O-08.

[14] S. Mathew et al., "Dye-Sensitized Solar Cells with 13% Efficiency Achieved through the Molecular Engineering of Porphyrin Sensitizers," *Nature Chem.*, vol. 6, 2014, pp. 242–247.

[15] K. Kakiage et al., "Highly-Efficient Dye-Sensitized Solar Cells with Collaborative Sensitization by Silyl-Anchor and Carboxy-Anchor Dyes," *Chem. Commun.*, vol. 51, 2015, pp. 15894–15897.

[16] M.A. Green et al., "Solar Cell Efficiency Tables (Version 49)," *Prog. Photovolt: Res. Appl.*, vol. 25, 2017, pp. 3–13.

[17] H. Pettersson et al., "Manufacturing Method for Monolithic Dye-Sensitized Solar Cells Permitting Long-Term Stable Low-Power Modules," *Sol. Energy Mater. Sol. Cells*, vol. 77, 2003, pp. 405–413.

[18] S. Dai et al., Design of DSC Panel with Efficiency More Than 6%," *Sol. Energy Mater. Sol. Cells*, vol. 85, 2005, pp. 447–455.

[19] R. Escalante et al., "Dye-Sensitized Solar Cell Scale-up: Influence of Substrate Resistance," *J. Renewable Sustainable Energy*, vol. 8, 2006, pp. 023704-1–023704-10.

[20] R. Sastrawan et al., "New Interdigital Design for Large Area Dye Solar Modules Using a Lead-Free Glass Frit Sealing," *Prog. Photovolt: Res. Appl.*, vol. 14, 2006, pp. 1625–1633.

[21] H. Seo et al., "The Fabrication of Efficiency-Improved W-Series Interconnect Type of Module by Balancing the Performance of Single Cells," *Sol. Energy*, vol. 83, 2009, pp. 2217–2222.

[22] Y.-D. Zhang et al., "How to Design Dye-Sensitized Solar Cell Modules," *Sol. Energy Mater. Sol. Cells*, vol. 95, 2011, pp. 2564–2569.

[23] L. Vesce et al., "Fabrication of Spacer and Catalytic Layers in Monolithic Dye-Sensitized Solar Cells," *J. Photovolt.*, vol. 3, 2013, pp. 1004–1011.

[24] F. Giordano et al., "A Realization of High Performance Large Area Z-series Interconnected Opaque Dye Solar Cell Modules," *Prog. Photovolt: Res. Appl.*, vol. 21, 2013, pp. 1653–1658.

[25] F. Giordano et al., "Series-Connection Designs for Dye Solar Cell Modules," *IEEE Trans. Electron Dev.*, vol. 58, 2011, pp. 2759–2764.

[26] M.W. Rowell and M.D. McGehee, "Transparent Electrode Requirements for Thin Film Solar Cell Modules," *Energy Environ. Sci.*, vol. 4, 2011, pp. 131–134.

[27] H. Hoppe, M. Seeland, and B. Muhsin, "Optimal Geometric Design of Monolithic Thin-Film Solar Modules: Architecture of Polymer Solar Cells," *Sol. Energy Mater. Sol. Cells*, vol. 97, 2012, pp. 119–126.

[28] K.-S. Lee, "Analytic Treatment of the Distributed Resistance of the Window Layer in Solar Cells with Parallel Grids," *Prog. Photovolt: Res. Appl.*, vol. 21, 2013, pp. 195–201.

[29] K.-S. Lee, "Analytic Formalism for Current Crowding in Light Emitting Diodes," *Phys. Status Solidi A*, vol. 209, no. 12, 2012, pp. 2630–2634.

[30] M. Ait Aouaj et al., "Comparative Study of ITO and FTO Thin Films Grown by Spray Pyrolysis," *Mater. Res. Bull.*, vol. 44, 2009, pp. 1458–1461.

[31] A. Hagfeldt et al., "Dye-Sensitized Solar Cells," *Chem. Rev.*, vol. 110, 2010, pp. 6595–6663.

[32] J. Halme et al., "Device Physics of Dye Solar Cells," *Adv. Energy Mater.*, vol. 22, 2010, pp. E210–E234.

[33] Y. Jun, J. Kim, and M.G. Kang, "A Study of Stainless Steel-Based Dye-Sensitized Solar Cells and Modules," *Sol. Energy Mater. Sol. Cells*, vol. 91, 2007, pp. 779–784.

[34] Y. Jun et al., "A Module of a TiO_2 Nanocrystalline Dye-Sensitized Solar Cell with Effective Dimensions," *J. Photochem. Photobiol. A: Chem.*, vol. 200, 2008, pp. 314–317.

Kyu-Seok Lee received his BS and MS degrees from Yonsei University, Seoul, Rep. of Korea and his PhD degree from Northeastern University, Boston, MA, USA, in 1979, 1981, and 1990, respectively, in physics. He was a research associate at Northeastern University (1990) and spent a postdoctoral year (1991–92) at the Institute of Physical and Chemical Researches in Saitama, Japan. He was with ETRI, Daejeon, Rep. of Korea as a researcher from 1992 until retirement in 2017. He served the ETRI Journal as the Editor-in-Chief (2008–12).

Man Gu Kang is a project manager at ETRI, Daejeon, Rep. of Korea and a professor at the University of Science and Technology, Daejeon, Rep. of Korea. He received his BS (1988), MS (1990), and PhD (2000) degrees in chemistry from Korea University, Seoul, Rep. of Korea. Since he moved to ETRI in 2000, he registered more than 100 domestic and international patents and authored 55 international articles related to dye-sensitized solar cells. One of his articles regarding flexible dye-sensitized solar cells based on metal substrates was selected as frontier work by the American Institute of Physics and American Physical Society in 2007. Currently, he is working on the fabrication of large area dye-sensitized solar cells for commercial applications.